

NINETEENTH EUROPEAN ROTORCRAFT FORUM

Paper n° H3

**EFFECTS OF BLADE FLEXIBILITY ON HELICOPTER
STABILITY AND FREQUENCY RESPONSE**

by

Stephen R. Turnour
Roberto Celi

Center for Rotorcraft Education and Research
Department of Aerospace Engineering
University of Maryland, College Park, MD 20742, USA

September 14-16, 1993
CERNOBBIO (Como)
ITALY

ASSOCIAZIONE INDUSTRIE AEROSPAZIALI
ASSOCIAZIONE ITALIANA DI AERONAUTICA ED ASTRONAUTICA

EFFECTS OF BLADE FLEXIBILITY ON HELICOPTER STABILITY AND FREQUENCY RESPONSE

Stephen R. Turnour¹
Roberto Celli²

Center for Rotorcraft Education and Research
Department of Aerospace Engineering
University of Maryland, College Park, USA

Abstract — This paper describes a methodology for the formulation of flight dynamic simulation models that include rotor blade flexibility. A coupled flap-lag-torsion elastic rotor model, previously used in aeroelasticity studies, is coupled with a blade-element type flight dynamic simulation model. The combined model is used to study the effects of elastic deformations of the main rotor blades on the trim, poles, step response, and frequency response characteristics of an articulated rotor helicopter in hover. The results clearly show that the modeling of blade flexibility has a very small effect on the dynamics of the helicopter in a wide range of frequencies that extend from 0.4-0.6 rad/sec to 50-55 rad/sec, at least in hover and for articulated rotor helicopters. The results also indicate that refining the main rotor model by including blade flexibility does not improve the prediction of the off-axis response to pilot inputs.

1. Introduction

In recent years there has been a growing interest in improving the fidelity of mathematical models of helicopter flight dynamics through a more accurate representation of the main rotor dynamics. The inclusion of rotor and inflow dynamics is necessary for a reliable design of high-gain flight control systems. Rotor models with adequate levels of detail are also needed to analyze the flight dynamics of hingeless and bearingless rotor helicopters, in which elastic deformations of the main rotor blades may have substantial effects on the handling qualities of the aircraft.

An important first step is the modeling of the dynamics of the individual main rotor blades, approximated as rigid bodies, possibly with root offsets and springs to simulate hingeless configurations. Several such models have been described in the literature. These include the Genhel model, originally formulated by Howlett [1], and later improved by Ballin [2], Diftler [3], and Kim *et al.* [4, 5], for the UH-60 Blackhawk, and by Kaplita *et al.* [6] for the CH-53. The Genhel rotor model was coupled with the aircraft model of the FLYRT rotor-map based simulation code, resulting in a coupled rotor-fuselage model that was specialized for the McDonnell Douglas AH-64 [7]. Other simulation models incorporating individual blade dynamics include those due to Curtiss [8], Chaimovich *et al.* [9], Miller and White [10], Talbot *et al.* [11], and the HELISTAB model developed by Padfield *et al.*. These models include some, or all, of the ingredients required for flight dynamics calculations, namely: calculation of the trim state of the helicopter, in straight or turning flight, extraction of linearized dynamic models, not necessarily limited to the 6 degree of freedom rigid body dynamics, and integration of the equations of motion to simulate the free flight response to arbitrary pilot inputs.

More recent work has focused on including rotor blade flexibility in the model. Although some comprehensive analyses used in industry and government laboratories contain several of the ingredients required for flight dynamic studies, only a very limited number of such studies has been reported in the literature. They are all based on the FLIGHTLAB model, originally developed by DuVal [12] by coupling the flexible rotor model of the REXOR aeroelastic analysis with the Genhel aircraft model [12]. The model was subsequently improved by He and Lewis [13] in the aerodynamic representation. Real-time execution speed is obtained through the use of parallel processing. While coupled flap-lag and uncoupled torsion dynamics are reported to be included, relatively few details of this rotor model have been presented. A validation study presented by

¹Graduate Research Assistant

²Associate Professor

Lewis [14] using UH-60 flight test data indicates that, for articulated rotor helicopters, the effect of blade flexibility is quite small in hover and increases slightly with increasing speed. Another study, focusing on the AH-64 [15], shows that a flexible blade model with higher order dynamic inflow may substantially improve the prediction of the off-axis response to pilot inputs.

In recent years there has also been growing interest in the formulation of helicopter dynamic models using the principles of multi-body dynamics (see, for example, Ref [16]). Using this approach, the helicopter is first considered as an assemblage of rigid and elastic independent bodies, the equations of motion of which are written with respect to a single inertial frame for the entire vehicle. Then the compatibility of the motions of these bodies is enforced through additional constraint equations that may be ordinary differential equations (ODE) and/or algebraic equations. The advantage of such formulation is the ease with which arbitrarily complex aircraft configurations can be modeled. The main disadvantages seem to be that the dimensionality of the mathematical model tends to increase substantially compared with traditional formulations, and that, at least for numerical time integrations, the selection of the solution algorithm requires greater care. In fact, if the constraint equations include algebraic equations, general purpose ODE solvers cannot be used, and special algorithms that can solve combined differential-algebraic systems need to be used instead. If the equations of motion are entirely in ODE form, general purpose ODE solvers again appear to be unsuitable, and special energy-conserving schemes should be used instead [16]. Whether the advantages of this new methodology outweigh its disadvantages remains a topic of discussion. No application of multibody dynamics based models to flight dynamics has been reported in the literature, although the methodology is well suited for the treatment of such problems.

The present paper has the following objectives:

1. To describe a methodology for the formulation and solution of flight dynamics simulation models that include a representation of the coupled flap-lag-torsional dynamics of elastic rotor blades. This methodology provides considerable flexibility in the modeling of aircraft and blade geometry and, although not as general as multibody dynamics, is entirely compatible with customary solution algorithms. This methodology is applied to the derivation of a nonreal-time flight simulation model that includes rotor flexibility. The level of detail of the rotor model described in this paper is that typical of aeroelastic analyses for isotropic rotor blades, and no simplifications or approximations are made for flight dynamics applications. Elastic coupling terms are rigorously retained, and nonlinearities due to "moderately" large elastic blade deflections are included in the model. The solution process includes: (i) trim in straight flight and coordinated, steady helical turns, (ii) extraction of high-order linearized models about arbitrary flight conditions, and (iii) integration of the nonlinear equations of motion of the helicopter, simulating free flight with arbitrary pilot inputs.
2. To present the results of a validation study carried out in the frequency domain using UH-60 hover flight test data.
3. To study the effect of rotor flexibility on the flight dynamic characteristics of an articulated rotor helicopter. Results are presented showing the effect of increasing number of modes on the trim state, the open loop poles, the free flight response to step inputs, and the frequency response characteristics of the helicopter in hover.

2. Mathematical Model

Overview

The mathematical model of the present study is basically the result of combining a rotor model previously used to study the aeromechanic characteristics of hingeless rotor helicopters [17] with the fuselage and inflow equations of the UM-Genhel model [5], and its trim, stability, and time integration solution algorithms. The formulation of several portions of the model has been discussed elsewhere in the literature, and only brief outlines will be provided here. The treatment of the inertia loads, and especially of acceleration dependent terms, on the other hand, will be presented in detail. In fact some issues concerning the treatment of these terms arise specifically in flight dynamics applications, and had not been dealt with in Refs. [5] and [17].

Fuselage

A rigid fuselage is assumed, and its motion is described by the nine nonlinear rigid body Euler equations. The states included in the model are:

$$u \ v \ w \ p \ q \ r \ \phi \ \theta \ \psi_F$$

(The subscript F has been added to ψ to avoid confusion with the blade azimuth angle.) The aerodynamic characteristics of fuselage and tail surfaces are provided in the form of tables of aerodynamic coefficients, obtained from wind tunnel tests and valid over a very wide range of angle of attack and sideslip [1]. Therefore, no small angle assumptions are invoked for the angles of attack of rotor and fuselage (within the range of validity of Euler angles). The delayed effects of rotor and fuselage downwash and sidewash on the tail surfaces are modeled through two first order equations. This adds two states to the model. Finally, a one state dynamic inflow model is used for the the tail rotor [5].

Main rotor blade model

The equations of motion are formulated using an "implicit" approach [18] in which all the various portions of the beam theory (such as the strain-displacement relations, the coordinate transformations from the undeformed to the deformed blade configuration, the stress-strain relations, etc.) are built *numerically* as part of the solution process. This approach eliminates the need for complex algebraic expansions of the various components of the nonlinear structural dynamic model of the blade, and is used for the calculation of the blade aerodynamic and inertia loads as well.

Structural and aerodynamic loads

The structural portion of the rotor blade model is identical to the model used in Ref. [18]. The rotor blades are modeled as Bernoulli-Euler beams undergoing coupled flap-lag-torsional motion. Small strains and moderate elastic deflections are assumed, introducing non-linearities in the equations of motion of the blade due to the kinematics of its deformation. A single load path at the blade root is assumed, therefore the present model is not suitable for the analysis of bearingless rotor configurations. A Drees type inflow model is used, and quasi-steady stall and compressibility effects are included through the use of look-up tables for the blade airfoils. Inflow dynamics is modeled through a three state [19] model.

Inertia loads

The main ingredient required for the calculation of the inertia loads is the acceleration of a generic point P of the blade. The position vector \mathbf{R}_P of the point P can be written as:

$$\mathbf{R}_P = \mathbf{R}_{CG} + \mathbf{R}_H + \mathbf{R}_B \quad (1)$$

where \mathbf{R}_{CG} is the position vector of the center of gravity (CG) of the helicopter with respect to a fixed point, \mathbf{R}_H is the position vector of the rotor hub with respect to the CG, and \mathbf{R}_B is the position vector of the point P with respect to the hub. The absolute velocity \mathbf{V}_P of the point is given by:

$$\mathbf{V}_P = \frac{d\mathbf{R}_P}{dt} = \frac{d\mathbf{R}_{CG}}{dt} + \frac{\partial\mathbf{R}_B}{\partial t} + \omega \times (\mathbf{R}_H + \mathbf{R}_B) \quad (2)$$

In Eq. (2) the velocity $\partial\mathbf{R}_H/\partial t$ of the hub as seen from the body axis system is equal to zero because the fuselage is assumed to be rigid, and ω is the angular velocity of the body axis system. The absolute acceleration \mathbf{a}_P of the point P is given by:

$$\begin{aligned} \mathbf{a}_P = \frac{d^2\mathbf{R}_P}{dt^2} &= \frac{d^2\mathbf{R}_{CG}}{dt^2} + \dot{\omega} \times \mathbf{R}_H + \omega \times (\omega \times \mathbf{R}_H) \\ &+ \frac{\partial^2\mathbf{R}_B}{\partial t^2} + \dot{\omega} \times \mathbf{R}_B + 2\omega \times \frac{\partial\mathbf{R}_B}{\partial t} + \omega \times (\omega \times \mathbf{R}_B) \end{aligned} \quad (3)$$

The first three terms in the equation represent the absolute acceleration of the hub, and the remaining four the acceleration of the point P with respect to the rotor hub. Furthermore, we have:

$$\frac{\partial\mathbf{R}_B}{\partial t} = \left(\frac{\partial\mathbf{R}_B}{\partial t} \right)_B + \boldsymbol{\Omega} \times \mathbf{R}_B \quad (4)$$

in which the notation $(\dots)_B$ denotes the velocity of the point P as seen by an observer rotating with the hub rotating coordinate system, and Ω is the main rotor speed. The corresponding acceleration is:

$$\frac{\partial^2 \mathbf{R}_B}{\partial t^2} = \left(\frac{\partial^2 \mathbf{R}_B}{\partial t^2} \right)_B + \dot{\Omega} \times \mathbf{R}_B + 2\Omega \times \left(\frac{\partial \mathbf{R}_B}{\partial t} \right)_B + \Omega \times (\Omega \times \mathbf{R}_B) \quad (5)$$

Combining Eqs. (3) and (5) results in the final expression for the absolute acceleration of a generic point P of the blade:

$$\begin{aligned} \mathbf{a}_P = & \frac{d^2 \mathbf{R}_{CG}}{dt^2} + \dot{\omega} \times \mathbf{R}_H + \omega \times (\omega \times \mathbf{R}_H) + \left(\frac{\partial^2 \mathbf{R}_B}{\partial t^2} \right)_B + \dot{\Omega} \times \mathbf{R}_B + 2\Omega \times \left(\frac{\partial \mathbf{R}_B}{\partial t} \right)_B \\ & + \Omega \times (\Omega \times \mathbf{R}_B) + \dot{\omega} \times \mathbf{R}_B + 2\omega \times \left[\left(\frac{\partial \mathbf{R}_B}{\partial t} \right)_B + \Omega \times \mathbf{R}_B \right] + \omega \times (\omega \times \mathbf{R}_B) \end{aligned} \quad (6)$$

A complete symbolic expansion of Eq. (6) is prohibitively complex, even when carried out using computerized symbolic manipulation, unless one uses an ordering scheme with rather restrictive assumptions on the magnitude of the fuselage motions. Such assumptions, that are largely incompatible with flight dynamics applications, are not necessary when a "numerical" formulation of the equations of motion is used. To illustrate the various steps of the procedure, the treatment of one of the terms, namely $2\omega \times (\Omega \times \mathbf{R}_B)$ will be described here in detail. The computer implementation of this acceleration term consists of:

$$\begin{aligned} 2\omega \times (\Omega \times \mathbf{R}_B) = & (g_{11} + g_{12}x_0 + g_{13}y_0 + g_{14}z_0) \hat{e}_x + \\ & (g_{21} + g_{22}x_0 + g_{23}y_0 + g_{24}z_0) \hat{e}_y + (g_{31} + g_{32}x_0 + g_{33}y_0 + g_{34}z_0) \hat{e}_z \end{aligned} \quad (7)$$

where:

$$\begin{aligned} g_{11} &= 2R_{21}\omega_y\Omega_z + 2R_{31}\omega_z\Omega_x - 2R_{11}\omega_y\Omega_y - 2R_{11}\omega_z\Omega_z \\ g_{12} &= 2R_{22}\omega_y\Omega_x + 2R_{32}\omega_z\Omega_x - 2R_{12}\omega_y\Omega_y - 2R_{12}\omega_z\Omega_z \\ &\vdots \\ g_{34} &= 2R_{14}\omega_x\Omega_z + 2R_{24}\omega_y\Omega_z - 2R_{34}\omega_x\Omega_x - 2R_{34}\omega_y\Omega_y \end{aligned}$$

The various terms appearing in the expressions above are the components of the position vector \mathbf{R}_B and of the angular velocity vectors ω and Ω , and are defined as follows:

$$\begin{aligned} \mathbf{R}_B = & (R_{11} + R_{12}x_0 + R_{13}y_0 + R_{14}z_0) \hat{e}_x + \\ & (R_{21} + R_{22}x_0 + R_{23}y_0 + R_{24}z_0) \hat{e}_y + (R_{31} + R_{32}x_0 + R_{33}y_0 + R_{34}z_0) \hat{e}_z \end{aligned} \quad (8)$$

$$\omega = \omega_x \hat{e}_x + \omega_y \hat{e}_y + \omega_z \hat{e}_z \quad (9)$$

$$\Omega = \Omega_x \hat{e}_x + \Omega_y \hat{e}_y + \Omega_z \hat{e}_z \quad (10)$$

The vectors $\hat{e}_x, \hat{e}_y, \hat{e}_z$ are the unit vectors of a rotating coordinate system, with \hat{e}_x aligned along the undeformed elastic axis of the blade, \hat{e}_y pointing forward, and \hat{e}_z pointing up. Equations (7) through (10) reflect the actual computer implementation of the component of the acceleration, and can accommodate a wide variety of rotor and fuselage geometries without modifications. For example, for a hingeless blade with a pitch hinge offset e_0 , and precone β_P , the position vector \mathbf{R}_B is defined as:

$$\mathbf{R}_B = e_0 \mathbf{i} + (x_0 + u) \hat{e}_x + v \hat{e}_y + w \hat{e}_z + y_0 \hat{e}'_x + z_0 \hat{e}'_y \quad (11)$$

The vectors $\hat{e}'_x, \hat{e}'_y, \hat{e}'_z$ are the unit vectors of a rotating coordinate system, with \hat{e}'_x tangent to the deformed elastic axis of the blade, \hat{e}'_y pointing forward, and \hat{e}'_z pointing up; x_0 is the blade spanwise coordinate, and $y_0 = \eta \cos \theta - \zeta \sin \theta$, and $z_0 = \eta \sin \theta + \zeta \cos \theta$, where η and ζ are coordinates measured along the principal axes of the cross section and θ is the blade geometric pitch angle.

After transforming all the components of \mathbf{R}_B to the $\hat{e}_x, \hat{e}_y, \hat{e}_z$ system, the coefficients R_{ij} in Eq. (8) can be identified as:

$$\begin{aligned} R_{11} &= e_0 + u & R_{12} &= 1 & R_{13} &= S_{21} & R_{14} &= S_{31} \\ R_{21} &= v & R_{22} &= 0 & R_{23} &= S_{22} & R_{24} &= S_{32} \\ R_{31} &= w - e_0\beta_P & R_{32} &= 0 & R_{33} &= S_{23} & R_{34} &= S_{33} \end{aligned} \quad (12)$$

The S_{ij} terms are components of the coordinate transformation matrix from the undeformed to the deformed blade coordinate system. Under the assumption of moderately large elastic deflections, and after using an ordering scheme, it is: $S_{21} = -(v_{,x} + \phi w_{,x})$, $S_{22} = 1$, $S_{23} = \phi$, $S_{31} = -(w_{,x} - \phi v_{,x})$, $S_{32} = -(\phi + v_{,x} w_{,x})$, $S_{33} = 1$. A numerical formulation of the S_{ij} terms that does not require the use of ordering schemes is presented in Ref. [18].

To obtain the components of the aircraft angular velocity vector ω in Eq. (9), first derive its components in a shaft fixed coordinate system, of unit vectors $\mathbf{i}_s, \mathbf{j}_s, \mathbf{k}_s$:

$$\omega = \omega_{x1}\mathbf{i}_s + \omega_{y1}\mathbf{j}_s + \omega_{z1}\mathbf{k}_s \quad (13)$$

$$\begin{aligned} \omega_{x1} &= p \cos \theta_s - r \sin \theta_s \\ \omega_{y1} &= p \sin \phi_s \sin \theta_s + q \cos \phi_s + r \sin \phi_s \cos \theta_s \\ \omega_{z1} &= p \cos \phi_s \sin \theta_s - q \sin \phi_s + r \cos \phi_s \cos \theta_s \end{aligned}$$

in which p, q, r are the customary roll, pitch, and yaw rates about the fuselage body axes, and θ_s and ϕ_s are the inclination angles of the mast, positive for a mast tilted back and to starboard. The components are then transformed to the hub nonrotating coordinate system, then to the hub rotating system, and finally to the undeformed blade system, with respect to which the components of ω are required:

$$\omega_x = -\omega_{x1} \cos \psi + \omega_{y1} \sin \psi + \beta_P \omega_{z1} \quad (14)$$

$$\omega_y = \omega_{y1} \cos \psi - \omega_{x1} \sin \psi \quad (15)$$

$$\omega_z = \beta_P \omega_{x1} \cos \psi - \beta_P \omega_{y1} \sin \psi + \omega_{z1} \quad (15)$$

where ψ is the blade azimuth angle. The coordinate transformations required to obtain Eq. (14) have been expanded symbolically in this case, but could easily be implemented numerically for blades of more complex geometry (e.g., with droop and sweep, or skewed flap or lag hinges). Finally, the components of the angular velocity vector $\Omega = \Omega \mathbf{k}$ of the main rotor are given by:

$$\Omega_x = \Omega \sin \beta_P \quad \Omega_y = 0 \quad \Omega_z = \Omega \cos \beta_P \quad (16)$$

This description of the treatment of the acceleration term $2\omega \times (\Omega \times \mathbf{R}_B)$ indicates that a numerical formulation of the equations of motion has two important benefits, namely:

1. Because the symbolic expansion of Eq. (6) is not required, one does not need to use ordering schemes to maintain the resulting algebraic expressions of a reasonable size. In particular, there is no need to limit the magnitude of the fuselage motions, which would be unduly restrictive for flight dynamics applications.
2. Various changes in blade and aircraft geometry can be accommodated with limited changes in computer implementation. For example, many changes in blade and hub geometry would simply require changes in Eqs. (11), (15), and (16), but not in Eqs. (7) through (10).

The numerical formulation of the equations of motion requires some modifications before it can be applied to flight dynamics. Because explicit symbolic expressions for the various elements of the mathematical model are never derived, the terms that contain the derivatives of the states are not available directly. This is not a problem in aeroelasticity applications because then both the steady-state response and the aeroelastic stability are calculated using linearized versions of the equations of motion, that can be built numerically using finite difference approximations [18]. In other words, the equations can be formulated in the generic form:

$$\mathbf{F}_{NL}(\mathbf{y}, \dot{\mathbf{y}}, \ddot{\mathbf{y}}; \psi) = \mathbf{0} \quad (17)$$

For flight dynamics applications, a formulation of the equations of motion of the type of Eq. (17) is still compatible with the solution algorithms commonly used for the trim problem, and for pole/zero and frequency response calculations. On the other hand, for the calculation of the free flight, nonlinear aircraft response to pilot inputs, one needs to have a formulation of the type:

$$\ddot{\mathbf{q}}^* = \mathbf{G}_{NL}(\mathbf{q}; \psi) \quad (18)$$

where $\mathbf{q} = [\mathbf{y}^T \ \dot{\mathbf{y}}^T]^T$ is the state vector. Therefore, not only must the $\ddot{\mathbf{q}}^*$ terms be identified and moved to the left-hand-side, but *all* such terms must be moved. In other words, the structure of the type $\ddot{\mathbf{q}}^* = \mathbf{G}_{NL}(\mathbf{q}, \dot{\mathbf{q}}; \psi)$, which typically arises from the formulation of the equations of motion, should be avoided because it complicates considerably time-marching solutions and the extraction of linearized models. This means that all the terms that are functions of the accelerations of the fuselage and the blade should be isolated. This can still be accomplished while maintaining all the advantages of the numerical formulation of the equations of motion. The mathematical model of this study is based on the assumption that the acceleration terms only appear in the inertia portion of the rotor equations of motion. Acceleration terms of aerodynamic origin are not considered here, but the same general treatment applies. The structural portion of the equations does not generate any acceleration terms.

The inertia terms proportional to $\ddot{\mathbf{q}}^*$ may only arise from the four terms underlined in Eq. (6). The first term, $d^2\mathbf{R}_{CG}/dt^2$, is the absolute acceleration of the CG of the helicopter, and contains terms proportional to the linear body accelerations $\ddot{u}, \ddot{v}, \ddot{w}$, and the angular accelerations $\ddot{p}, \ddot{q}, \ddot{r}$. The second and fourth terms, that is $\dot{\omega} \times \mathbf{R}_H$ and $\dot{\omega} \times \mathbf{R}_B$, contain terms proportional to $\ddot{p}, \ddot{q}, \ddot{r}$. The details of the manipulations required to isolate these terms are not presented here for reasons of space, but are straightforward and quite similar to those outlined above for the derivation of the sample term $2\omega \times (\Omega \times \mathbf{R}_B)$. It should also be pointed out that all these terms are linear in the components of the vector $\ddot{\mathbf{q}}^*$. Therefore they can be obtained by calculating numerically the derivatives of the acceleration with respect to each component of the $\ddot{\mathbf{q}}^*$ vector, using finite difference approximations. Because of the linearity in $\ddot{\mathbf{q}}^*$ these derivatives will be exact regardless of the size of the finite difference step. This alternate approach is quite simple to implement, although it is time consuming because the finite difference calculations need to be repeated at each blade azimuth angle. The third underlined term in Eq. (6), $(\partial^2\mathbf{R}_B/\partial t^2)_B$, also generates terms proportional to $\ddot{\mathbf{q}}^*$ because it involves the second derivatives with respect to time of the S_{ij} terms in Eq. (12) and therefore it involves the blade accelerations. For example, the \hat{e}_x component of the third term is obtained by differentiating Eq. (8) (specialized using Eq. (12)) twice with respect to time:

$$\left(\frac{\partial^2 \mathbf{R}_B}{\partial t^2} \right)_B \cdot \hat{e}_x = \left[\ddot{u} + \left(\ddot{S}_{21} + \ddot{\theta} S_{31} + 2\dot{\theta} \dot{S}_{31} - \dot{\theta}^2 S_{21} \right) y_0 + \left(\ddot{S}_{31} - \ddot{\theta} S_{21} - 2\dot{\theta} \dot{S}_{21} - \dot{\theta}^2 S_{31} \right) z_0 \right] \quad (19)$$

The underlined terms contain terms proportional to $\ddot{\mathbf{q}}^*$ and need to be moved to the left-hand-side of the equations of motion. In other words:

$$\begin{aligned} \left(\frac{\partial^2 \mathbf{R}_B}{\partial t^2} \right)_B \cdot \hat{e}_x \Big|_{LHS} &= \left[\ddot{u} + \ddot{S}_{21} y_0 + \ddot{S}_{31} z_0 \right] \\ &= \ddot{u} + \left[\ddot{S}_{21} (\cos \theta + \sin \theta) \right] \eta + \left[\ddot{S}_{31} (\cos \theta - \sin \theta) \right] \zeta \end{aligned} \quad (20)$$

For the calculation of the inertia forces, the components of the acceleration are multiplied by the blade mass density ρ and integrated over the area A of the cross section of the blade. All the terms in the previous expression are constant over the cross section, except for η and ζ . Then we have:

$$\int_A \rho \eta \, dA = m x_I \quad \int_A \rho \zeta \, dA = 0$$

for a symmetric cross-section. This suggests that the \ddot{S}_{ij} terms are small enough compared with \ddot{u}, \ddot{v} , and \ddot{w} that they can safely be neglected in flight dynamics applications.

3. Solution process

The nonlinear, partial differential equations of motion of the rotor blades are transformed into ODEs by eliminating the spanwise coordinate as an independent variable using a finite element Galerkin method [18]. The blades are assumed to have identical properties, but may have different motions. The number of blade degrees of freedom arising from the finite element discretization is reduced through a modal coordinate transformation based on the coupled flap-lag-torsion modes of the blade, isolated from the fuselage. The modal coordinate transformation also provides the means for the assembly of the blade structural, inertia, and aerodynamic loads. The corresponding nodal load vectors for each finite element are multiplied by the portion of the normal mode matrix that corresponds to that element, and the transformed modal load vectors are assembled by directly summing them. Individual mass, damping, and stiffness matrices are never directly built in the process. The equations of motion of the blades are formulated in the rotating system, and the solution is also carried out in the rotating system. A multiblade coordinate transformation is performed prior to the output of the results, so that all the results generated by the computer code implementing this model are in the nonrotating aircraft body axis system.

The state vector in the nonrotating coordinate system is defined as:

$$\mathbf{q}_F = [u \ v \ w \ p \ q \ r \ \phi \ \theta \ \psi \ q_0^1 \ q_{1c}^1 \ q_{1s}^1 \ q_2^1 \ q_0^1 \ q_{1c}^1 \ q_{1s}^1 \ q_2^1 q_0^2 \ q_{1c}^2 \ q_{1s}^2 \ q_2^2 \ q_0^2 \ q_{1c}^2 \ q_{1s}^2 \ q_2^2 \\ \dots q_0^m \ q_{1c}^m \ q_{1s}^m \ q_2^m \ q_0^m \ q_{1c}^m \ q_{1s}^m \ q_2^m \nu_0 \ \nu_{1c} \ \nu_{1s} \ \nu_{0T} \ \lambda_H \ \lambda_S]^T \quad (21)$$

in which q_0^k , q_{1c}^k , q_{1s}^k , and q_2^k are respectively the components of the k -th generalized coordinate for all the blades of a 4-bladed rotor in the nonrotating system, with $k = 1, 2, \dots, m$.

The first step of the solution process is the calculation of the trim state of the helicopter. The flight condition is defined by airspeed, turn rate, and climb angle. Straight and level flight conditions, including hover, are therefore treated as a special case of turning flight. The trim procedure, which is an extended version of Chen's procedure [20] is described in detail in Ref. [5]. The unknowns of the trim problem are: the steady state values of main rotor and tail rotor pitch controls, angle of attack α and sideslip β of the fuselage, average inflow over the main and the tail rotor disks, fuselage pitch and roll attitude angles θ and ϕ , and roll, pitch, and yaw rates p , q , and r . The trim solution also provides the steady state periodic motion of the blades in flap, lag, and torsion in the form of a truncated Fourier series for the quantities q in Eq. (21). These quantities also define the equilibrium position of the helicopter, about which linearization of the equations of motion is carried out.

Because the equations of motion of the system are written in rigorous first-order form, Eq. (18), linearized state and control matrices can be obtained by perturbing the equations of motion, one state or control at a time, and using finite difference approximations. The rotor states are defined in the rotating system, therefore the corresponding portions of the linearized system and control matrices are transformed to the body fixed coordinate system using multiblade coordinate transformations. The final matrices correspond to the state vector \mathbf{q}_F defined in Eq. (21). The linearization generates matrices of an order equal to the number of elements of the full state vector \mathbf{q}_F . Reduced order matrices can be obtained by assuming that the states to be dropped have an infinitely fast dynamics, setting their derivatives equal to zero, and condensing them out [21].

Finally, free-flight response to arbitrary pilot inputs is simulated by integrating numerically the equations of motion of the helicopter, symbolically written in Eq. (21). The solution method is a variable-step, variable-order Adams-Bashforth algorithm.

4. Results

All the results presented in this section refer to a Sikorsky UH-60 helicopter in hover at an altitude of 200 feet and a gross weight of 15334 lbs, with the flight control system turned off (bare airframe configuration). The results are intended to show the effect of blade flexibility on trim, poles, frequency response, and response to control inputs. In all cases each rotor blade is modeled using four finite elements. The outermost element models the swept tip approximately, through equivalent offsets of the aerodynamic center and center of mass of the cross sections with respect to

the elastic axis, assumed to be straight for the entire blade. Three finite elements of equal length model the straight portion of the blade.

The first five rotating natural frequencies and corresponding mode shapes of the blade are shown in Figure 1. In order of increasing natural frequency the first and second modes are respectively a rigid body lag mode with natural frequency of 0.27/rev, and a rigid body flap mode with natural frequency of 1.035/rev. The main rotor speed is 27 rad/sec. In the model presented in this paper, the treatment of rigid body and elastic modes is identical, that is a rigid body mode is treated as a special case of elastic mode with a mode shape consisting of a straight line. This treatment is not rigorously correct. If an order of magnitude analysis is carried out, by assuming that rigid body flap and lag displacements, nondimensionalized by the blade radius, and their velocities, nondimensionalized by hover tip speed, are of order $O(\epsilon)$ with $\epsilon \approx 0.1 - 0.2$, then the error consists of neglecting terms of order $O(\epsilon^2)$ compared to terms of order $O(1)$. Therefore the error is quite small, and certainly acceptable in light of the overall accuracy of the mathematical model. Thus, all the results marked with "2 modes" indicate a rigid blade blade model, with no effects of rotor flexibility retained. The third mode is the first elastic mode, and has a frequency of 2.82/rev. This is mainly a flap mode, but because of the coupling introduced by the blade geometry (e.g. the swept tip) there is a substantial torsion component. The fourth mode, and second elastic mode, is a lag mode of frequency 4.80/rev. The fifth mode, and third elastic mode, has a frequency of 4.94/rev and is mainly a torsion mode with a small flap component.

Table 1 shows the predicted trim values with the rotor modeled using up to 5 modes. For the purpose of calculating the steady-state equilibrium position of the blades, each mode is expanded in a three harmonic Fourier series. Therefore the total number of algebraic equations and unknowns of the trim problem is equal to 14 plus 7 per blade mode, for a total that ranges from 28 for a rotor model with rigid blades to 49 for two rigid and three elastic modes. No convergence problems were observed as the size of the system of nonlinear algebraic trim equations increased. Blade flexibility has a very small effect on the trim state in hover. The largest change is a variation of about 4% in the lateral cyclic pitch. The largest variation occurs when adding the fifth mode, which is mainly a torsion mode. A smaller variation occurs when adding the third mode, which is mainly an elastic flap mode, with some torsion contribution. This indicates that the change in lateral cyclic is probably due to the redistribution of lift across the rotor disk due to the elastic torsional deformations.

Table 2 shows the damping ratio ζ of each mode. It is clear from the table that the addition of blade flexibility has a very small effect on the prediction of the fixed-stick stability characteristics of the helicopter. Typical variations from two modes (rigid blades) to five are typically of 1-2% or less. The only significant variation in damping ratio occurs for the phugoid mode. When one elastic flap mode is added to the model, the magnitude of the (negative) damping doubles, probably due to the changed dynamics of the rotor tiltback phenomenon. Further additions of a lag elastic mode and a mostly torsion elastic mode increase the predicted strength of the instability by a smaller amount.

The time history of the response to a 1 inch lateral step input is shown in Figure 2. The Figure shows the response in the three linear velocities and the three angular velocities. Very little effect of blade flexibility appears from all the plots. Small changes are visible in the time histories of q and u , indicating that including blade flexibility leads to predicting a slightly higher acceleration. This is probably due to small changes in flapping dynamics, that may also cause the changes in phugoid stability previously mentioned. More importantly, the results shown in Figure 2 (and those for step inputs of the other controls, not presented here) indicate that the problems often encountered in predicting the off-axis response to pilot inputs in hover are not due to the lack of modeling of rotor flexibility, and that the actual cause must be found elsewhere.

The bare airframe frequency responses to pilot control inputs are presented in Figures 3 through 5 for lateral, longitudinal, and collective respectively. Each Figure shows magnitude and phase plots for various numbers of modes, as well as magnitude and phase identified from flight test data. The portions of the Bode plots in the frequency band of interest in rotor dynamics are also shown enlarged in each Figure. The plots indicate that the main effect of blade flexibility on the frequency response occurs at frequencies above 50-60 rad/sec, corresponding to about 2/rev. This is not unexpected, because such higher frequencies are in the area of the flexible blade modes. Some effects also appear at very low frequencies, of 0.5 rad/sec and below. These are probably associated with the redistribution of aerodynamic loads across the rotor disk due to the torsional deformations of

the blade, and to the slight changes in tip-path-plane dynamics due to the elastic flap deformations of the blades. Unfortunately, coherence estimates indicate that the experimental data are rather unreliable precisely in these higher and lower frequency bands. Therefore it is not possible to determine whether the introduction of blade flexibility modeling improves the correlation with experiment. In the frequency band from 0.5-1 rad/sec to 10-20 rad/sec the effect of blade flexibility is minimal. The overall agreement with flight test data in this frequency band is reasonably good.

Finally, Figures 6 and 7 show two examples of bare airframe, off-axis frequency responses, namely pitch rate q due to lateral cyclic and roll rate p due to longitudinal cyclic. Coherence estimates indicate that the flight test data may be questionable at all frequencies in the first case, and should be reliable between 2 and 20-25 rad/sec in the second case. As in the on-axis response, the effects of blade flexibility are noticeable only at high frequencies, above 2-3/rev, and very low frequencies, below 0.3-0.4 rad/sec. For intermediate frequencies, if one assumes the overall correctness of the flight test data, the amplitude correlation is reasonably good, and the overall features of the magnitude plots are captured by the model. On the other hand, the phase prediction is poor, with a difference between predicted and actual phase delays of about 180 degrees over a fairly wide band of frequencies. Clearly, neglecting the elastic deformations of the blade is not the reason for the discrepancy, at least in hover and for this particular helicopter configuration.

5. Summary and Conclusions

A methodology for the formulation of flight dynamic simulation models that include rotor blade flexibility was described in this paper. This methodology, successfully applied in aeroelasticity research, consists of using features of the solution process to reduce to a minimum the amount of symbolic algebraic manipulation required to formulate the equations of motion, and results in very flexible and modular implementations. A coupled flap-lag-torsion elastic rotor model, previously used in aeroelasticity studies, was coupled with a blade-element type flight dynamic simulation model. The combined model was used to study the effects of elastic deformations of the main rotor blades on the trim, poles, step response, and frequency response characteristics of an articulated rotor helicopter in hover.

For this particular helicopter configuration and flight condition, the results clearly show that the modeling of blade flexibility has a very small effect on the dynamics of the helicopter in a wide range of frequencies that extend from 0.4-0.6 rad/sec to 50-55 rad/sec. Above these frequencies, corresponding to about 2/rev, significant effects appear, but these frequencies are well beyond the frequencies of interest in flight mechanics unless very high-gain flight control systems are used. At low frequencies some effects appear, in the frequency response and the phugoid characteristics. These effects are probably due to the redistribution of aerodynamic loads over the rotor disk caused by the elastic torsional deformations of the blades, and to small changes in tip path plane dynamics due to the elastic flapping motion of the blades. The results presented in this paper indicate that refining the main rotor model by including blade flexibility does not improve the prediction of the off-axis response to pilot inputs, at least in hover and for articulated rotor helicopters.

References

- [1] Howlett, J.J., "UH-60A Black Hawk Engineering Simulation Program—Volume II—Mathematical Model," NASA CR-166309, Dec. 1981.
- [2] Ballin, M.G., "Validation of a Real-Time Engineering Simulation of the UH-60A Helicopter," NASA TM-88360, Feb. 1987.
- [3] Diftler, M.A., "UH-60A Helicopter Stability Augmentation Study," Paper No. 74, *Proceedings of the Fourteenth European Rotorcraft Forum*, Milano, Italy, Sept. 1988.
- [4] Kim, F.D., Celi, R., and Tischler, M.B., "High-Order State Space Simulation Models of Helicopter Flight Mechanics," *Proceedings of the Sixteenth European Rotorcraft Forum*, Glasgow, Scotland, Sept. 1990, to appear in the *Journal of the American Helicopter Society*.

- [5] Kim, F.D., Celi, R., and Tischler, M.B., "Forward Flight Trim and Frequency Response Validation of a Helicopter Simulation Model," *Proceedings of the 47th Annual Forum of the American Helicopter Society*, Phoenix, Arizona, May 1991, pp. 155-168, to appear in the *Journal of Aircraft*.
- [6] Kaplita, T.T., Driscoll, J.T., Diftler, M.A., and Wong, S.W., "Helicopter Simulation Development by Correlation with Frequency Sweep Flight Test Data," *Proceedings of the 45th Annual Forum of the American Helicopter Society*, Boston, MA, May 1989, pp. 681-692.
- [7] Mansur, M.H., Tischler, M.B., Chaimovich, M., Rosen, A., and Rand, O., "Modeling Methods for High-Fidelity Rotorcraft Flight Mechanics Simulation," *Proceedings of the Sixteenth European Rotorcraft Forum*, Glasgow, Scotland, Sept. 1990.
- [8] Zhao, X., and Curtiss, H.C., "A Linearized Model of Helicopter Dynamics Including Correlation With Flight Test," Second International Conference on Rotorcraft Basic Research, University of Maryland, College Park, MD, Feb. 1988.
- [9] Chaimovich, M., Rosen, A., and Rand, O., "A Generic Harmonic Rotor Model for Helicopter Flight Simulation," *Proceedings of the Seventeenth European Rotorcraft Forum*, Berlin, Germany, Sept. 1991, pp. 351-364.
- [10] Miller, D.G., and White, F., "A Treatment of the Impact of Rotor-Fuselage Coupling on Helicopter Handling Qualities," *Proceedings of the American Helicopter Society 43rd Annual Forum*, St. Louis, Missouri, May 1987.
- [11] Talbot, P.D., Tinling, B.E., Decker, W.A., and Chen, R.T.N., "A Mathematical Model of a Single Main Rotor Helicopter for Piloted Simulation," NASA TM-84281, Sept. 1982.
- [12] DuVal, R., "A Real-Time Blade Element Helicopter Simulation for Handling Qualities Analysis," *Fifteen European Rotorcraft Forum*, Paper No. 59, Amsterdam, September 1989.
- [13] He, C., and Lewis, W. D., "A Parametric Study of Real Time Mathematical Modeling Incorporating Dynamic Wake and Elastic Blades," *Proceedings of the 48th Annual Forum of the American Helicopter Society*, Washington, D.C., June 1992, pp. 1181-1196.
- [14] Lewis, W. D., "An Aeroelastic Model Structure Investigation for a Manned Real-Time Rotorcraft Simulation," *Proceedings of the 48th Annual Forum of the American Helicopter Society*, St. Louis, MO, May 1993, pp. 391-418.
- [15] Sturisky, S.H., and Schrage, D.P., "System Identification Validation of an AH-64 Aeroelastic Simulation Model," *Proceedings of the 48th Annual Forum of the American Helicopter Society*, St. Louis, MO, May 1993, pp. 481-504.
- [16] Bauchau, O. A., and Kang, N. K., "A Multibody Formulation for Helicopter Structural Dynamic Analysis," *Journal of the American Helicopter Society*, Vol. 38, No. 2, April 1993, pp. 3-14.
- [17] Spence, A., and Celi, R., "Coupled Rotor-Fuselage Dynamics in Turning Flight," *Proceedings of the AIAA Dynamics Specialist Conference*, Dallas, Texas, April 1992, pp. 292-301.
- [18] Celi, R., "Helicopter Rotor Blade Aeroelasticity in Forward Flight with an Implicit Structural Formulation," *AIAA Journal*, Vol. 30, No. 9, September 1992, pp. 2274-2282.
- [19] Pitt, D.M., and Peters, D.A., "Theoretical Prediction of Dynamic Inflow Derivatives," *Vertica*, Vol. 5, No. 1981, pp. 21-34.
- [20] Chen, R.T.N., and Jeske, J.A., "Kinematic Properties of the Helicopter in Coordinated Turns," NASA Technical Paper 1773, Apr. 1981.
- [21] Padfield, G. D., "On the Use of Approximate Models in Helicopter Flight Mechanics," *Vertica*, Vol. 5, 1981.

Trim Variable	5 Modes	4 Modes	3 Modes	2 Modes
θ_{1c} - Lateral Cyclic (deg)	-0.8030853	-0.7753428	-0.7720500	-0.7678738
θ_{1s} - Longitudinal Cyclic (deg)	-2.2538149	-2.3246086	-2.3235615	-2.3454271
θ_0 - Collective (deg)	19.4771914	19.6472625	19.6524371	19.6669182
θ_t - Tail Rotor Collective (deg)	26.0941130	26.0038843	25.9935800	25.9946443
α - Aero Angle of Attack (deg)	4.12903096	4.12872817	4.14674293	4.15444505
β - Sideslip Angle (deg)	0.00000000	0.00000000	0.00000000	0.00000000
ϕ - Fus. Roll Attitude (deg)	-3.3707576	-3.3729341	-3.3770570	-3.4325666
θ - Fus. Pitch Attitude (deg)	4.12191225	4.12160078	4.1395671	4.14721806
ν_0 - Constant Inflow	0.05731249	0.05731283	0.05731327	0.05731323
ν_{1c} - 1st Harm. Cos. Inflow	0.00185462	0.00185342	0.00183632	0.00182987
ν_{1s} - 1st Harm. Sin. Inflow	0.00123527	0.00123546	0.00123828	0.00123915
ν_t - Tail Rotor Inflow	0.09841323	0.09840366	0.09842084	0.09841497
ν_x - Fuselage Downwash	0.08468736	0.08470459	0.08477197	0.08478088
ν_y - Fuselage Sidewash	-1.8000000	-1.8000000	-1.8000000	-1.8000000
q10 - 1st Mode Const.	-0.1714281	-0.1708484	-0.1709462	-0.1697369
q11c - 1st Mode 1st Cos.	-0.0008454	-0.0008437	-0.0008940	-0.0009020
q11s - 1st Mode 1st Sin.	0.00181240	0.00179769	0.00148620	0.00146773
q12c - 1st Mode 2nd Cos.	-0.0002793	-0.0002795	-0.0002972	-0.0002897
q12s - 1st Mode 2nd Sin.	-0.0002394	-0.0002380	-0.0001991	-0.0002018
q13c - 1st Mode 3rd Cos.	-0.0000054	-0.0000054	0.00000491	0.00000443
q23s - 1st Mode 3rd Sin.	0.00000334	0.00000296	0.00000569	0.00000599
q20 - 2nd Mode Const.	0.05592063	0.05582125	0.05581857	0.05575930
q21c - 2nd Mode 1st Cos.	0.01142070	0.01150162	0.01160786	0.01127529
q21s - 2nd Mode 1st Sin.	0.03408331	0.03398172	0.03382628	0.03369054
q22c - 2nd Mode 2nd Cos.	0.00002421	0.00002074	0.00001063	0.00001602
q22s - 2nd Mode 2nd Sin.	0.00000114	0.00001210	0.00001477	0.00002261
q23c - 2nd Mode 3rd Cos.	0.00000245	0.00000374	0.00000062	0.00000036
q23s - 2nd Mode 3rd Sin.	0.00000036	0.00000093	0.00000137	-0.00000000
q30 - 3rd Mode Const.	-0.0009452	-0.0010900	-0.0010130	
q31c - 3rd Mode 1st Cos.	-0.0005388	-0.0005556	-0.0003940	
q31s - 3rd Mode 1st Sin.	-0.0000538	-0.0000444	0.00003918	
q32c - 3rd Mode 2nd Cos.	0.00007785	0.00008141	0.00006210	
q32s - 3rd Mode 2nd Sin.	0.00002479	0.00002121	-0.0000362	
q33c - 3rd Mode 3rd Cos.	-0.0000203	-0.0000180	-0.0000208	
q33s - 3rd Mode 3rd Sin.	0.00004059	0.00003758	-0.0000095	
q40 - 4th Mode Const.	0.00009330	0.00012309		
q41c - 4th Mode 1st Cos.	0.00024502	0.00024956		
q41s - 4th Mode 1st Sin.	0.00009771	0.00009106		
q42c - 4th Mode 2nd Cos.	-0.0000412	-0.0000420		
q42s - 4th Mode 2nd Sin.	-0.0000469	-0.0000463		
q43c - 4th Mode 3rd Cos.	-0.0147017	-0.0000150		
q43s - 4th Mode 3rd Sin.	-0.0000039	-0.0000034		
q50 - 5th Mode Const.	-0.0028306			
q51c - 5th Mode 1st Cos.	-0.0000092			
q51s - 5th Mode 1st Sin.	0.00000697			
q52c - 5th Mode 2nd Cos.	0.00004191			
q52s - 5th Mode 2nd Sin.	-0.0000383			
q53c - 5th Mode 3rd Cos.	-0.0000121			

Table 1: Trim state of the helicopter in hover.

No.	Mode Type	5 Modes	4 Modes	3 Modes	2 Modes
1	Heading	0.000	0.000	0.000	0.000
2,3	Progressive Flap	0.223	0.219	0.224	0.224
4	Tail Rotor Inflow	1.000	1.000	1.000	1.000
5,6	Progressive Lag	0.279	0.279	0.208	0.207
7,8	Regressive Flap	0.992	0.991	0.992	0.992
9,10	Reactionless Flap	0.457	0.451	0.457	0.458
11,12	Collective Flap	0.426	0.416	0.426	0.427
13,14	Regressive Lag	0.195	0.198	0.187	0.188
15	Main Rotor Inflow	1.000	1.000	1.000	1.000
16	Collective Lag	1.000	1.000	1.000	1.000
17	Collective lag	1.000	1.000	1.000	1.000
18,19	Reactionless Lag	0.811	0.797	0.802	0.799
20	Inflow Harmonics	1.000	1.000	1.000	1.000
21,22	Short Period	0.929	0.931	0.910	0.913
23	Roll rate	1.000	1.000	1.000	1.000
24,25	Dutch Roll	0.080	0.079	0.101	0.090
26	Spiral	-1.000	-1.000	-1.000	-1.000
27,28	Phugoid	-0.182	-0.191	-0.151	-0.073
29	Delayed Downwash	1.000	1.000	1.000	1.000
30	Delayed Sidewash	1.000	1.000	1.000	1.000
31	Inflow Harmonics	1.000	1.000	1.000	1.000
32,33	Progress Flap Bending	0.137	0.143	0.094	
34,35	Collective Flap Bending	0.155	0.163	0.124	
36,37	Reactionless Flap Bend	0.201	0.209	0.125	
38,39	Regress Flap Bending	0.238	0.249	0.183	
40	Lag-Lag Bending Regress	1.000	1.000		
41	Progress Lag Bending	1.000	1.000		
42	Progress Lag Beinding	1.000	1.000		
43,44	Regress Lag Bending	0.525	0.506		
45,46	Reactionless Lag Bending	0.789	0.797		
47,48	Collective Lag Bending	0.751	0.766		
49,50	Regressive Torsion	0.045			
51,52	Collective Torsion	0.053			
53,54	Reactionless Torsion	0.056			
55,56	Progressive Torsion	0.066			

Table 2: Damping ratio ζ of each mode for the helicopter in hover. Two numbers in the first column denote a complex conjugate pair. A damping ratio of ± 1 denotes a pole on the real axis.

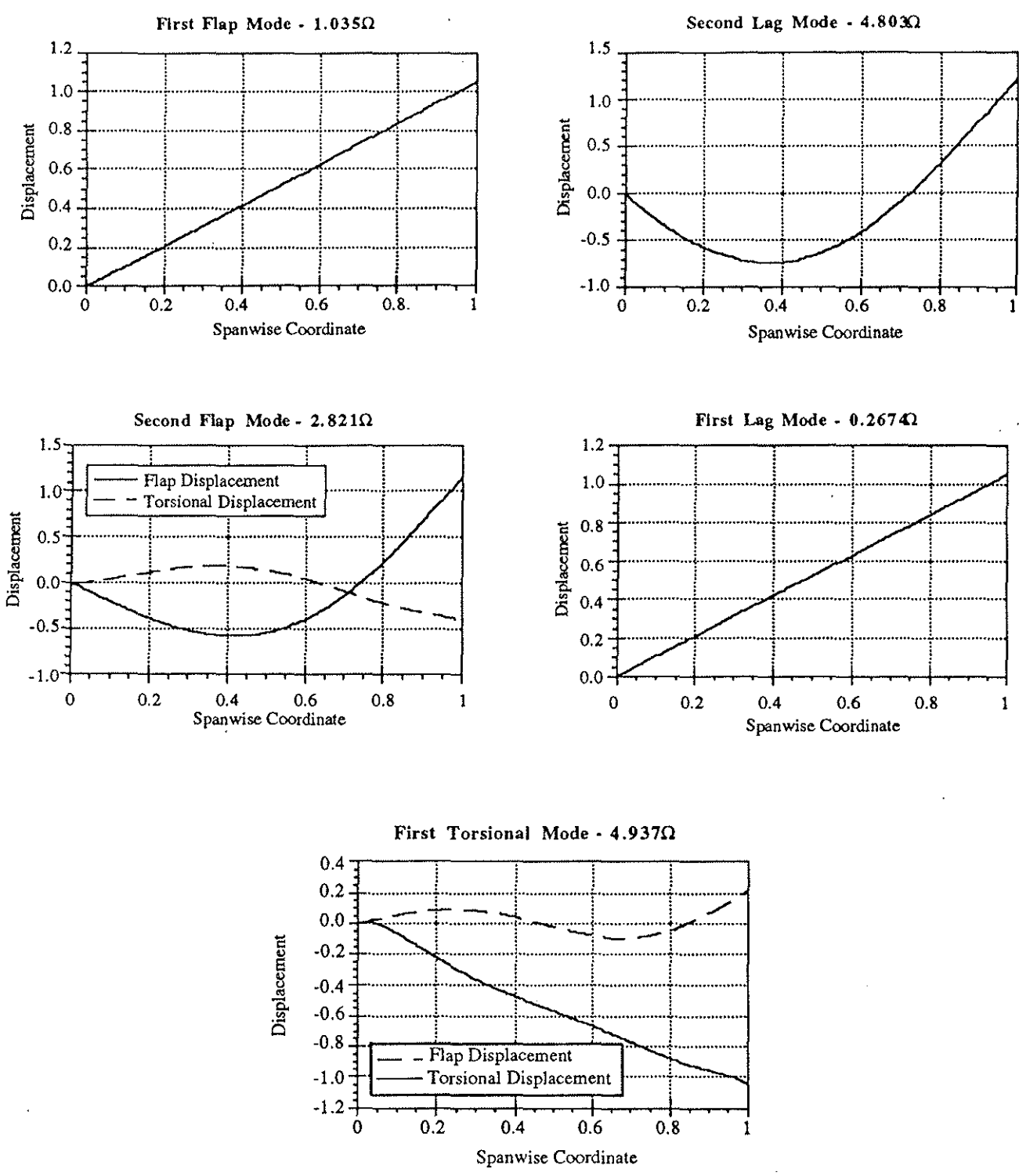


Figure 1: Natural frequencies and mode shapes of main rotor blade.

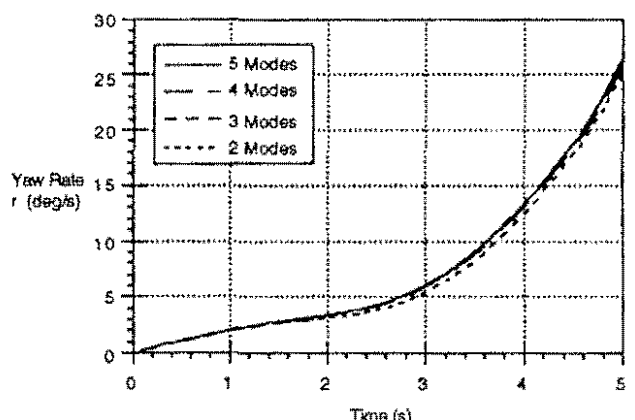
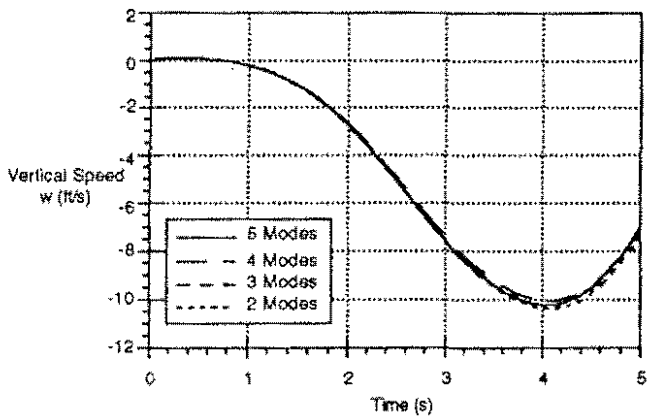
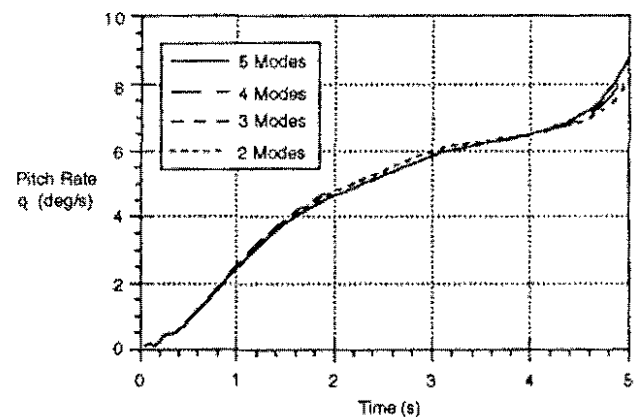
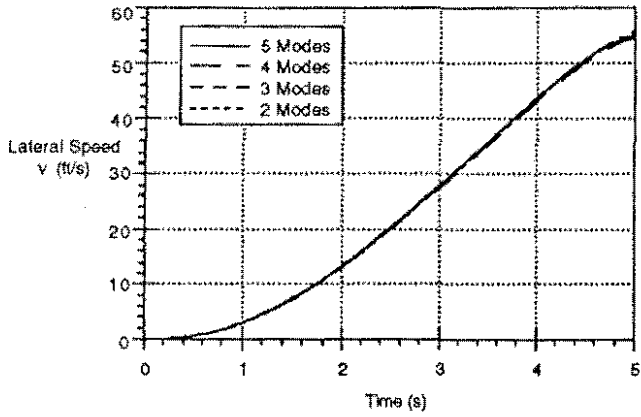
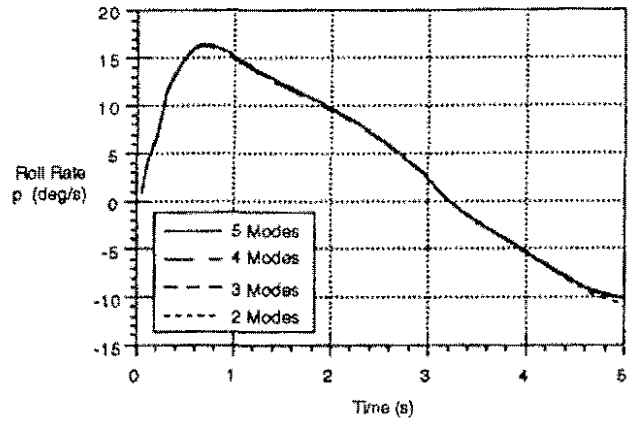
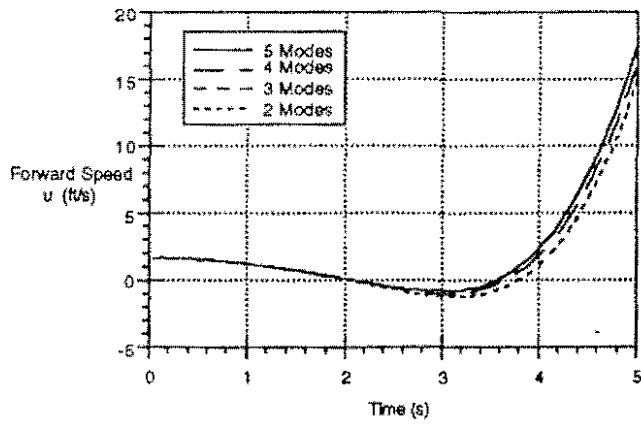


Figure 2: Time histories of the response to a 1-inch step input of lateral cyclic pitch.

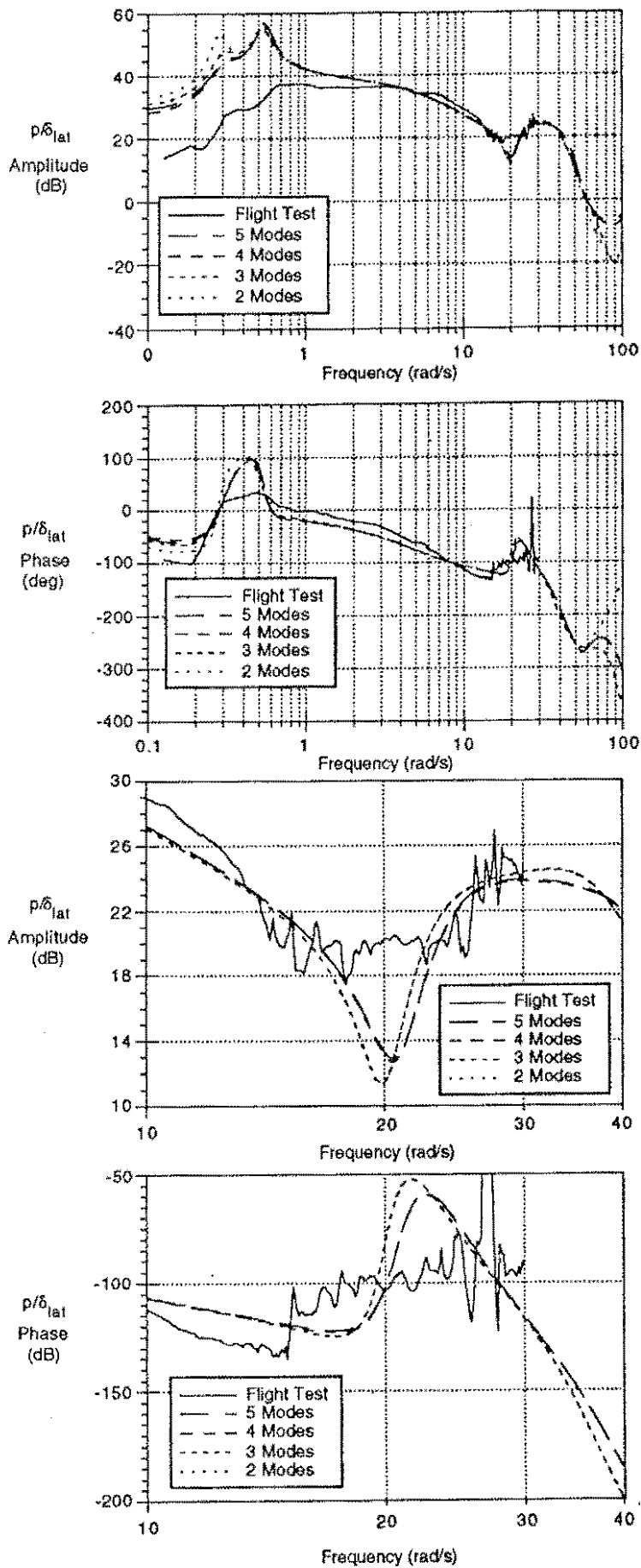


Figure 3: Roll rate frequency response to lateral cyclic input δ_{lat} .

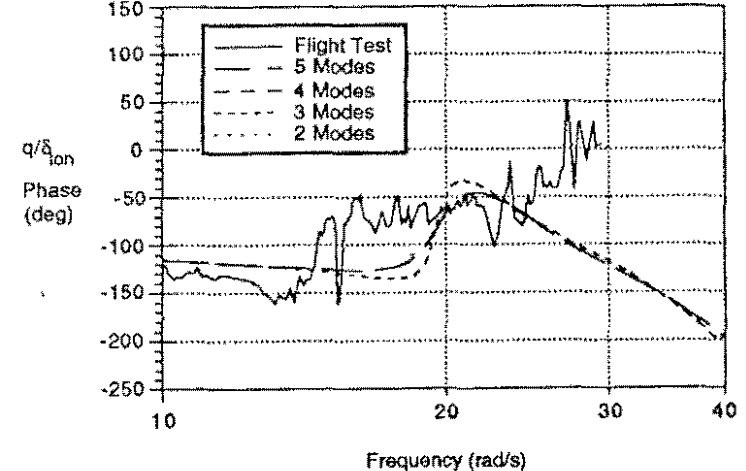
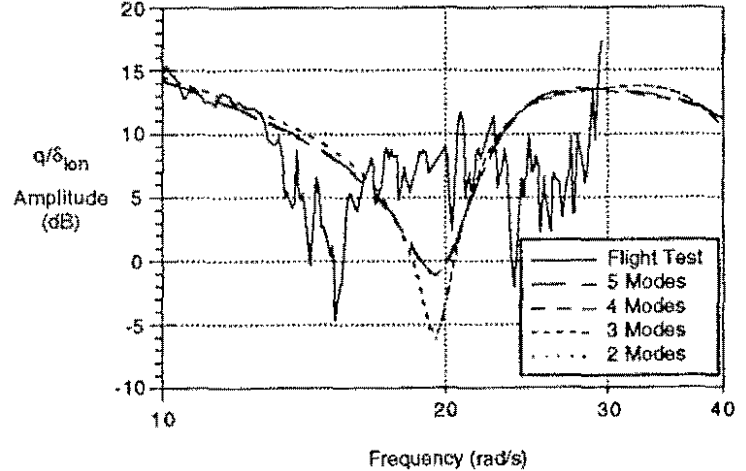
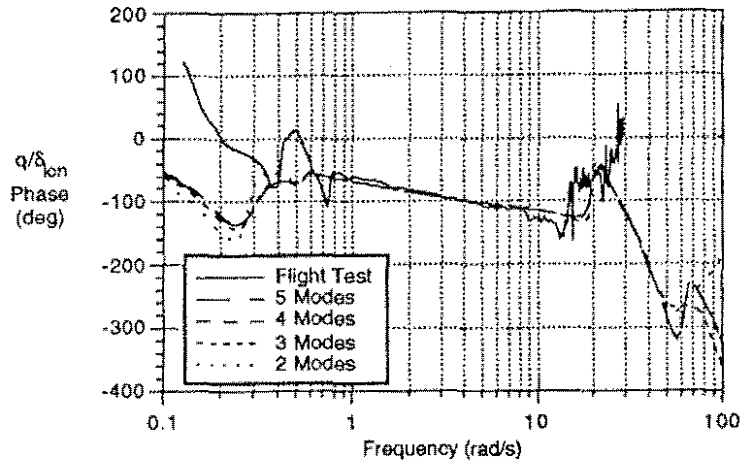
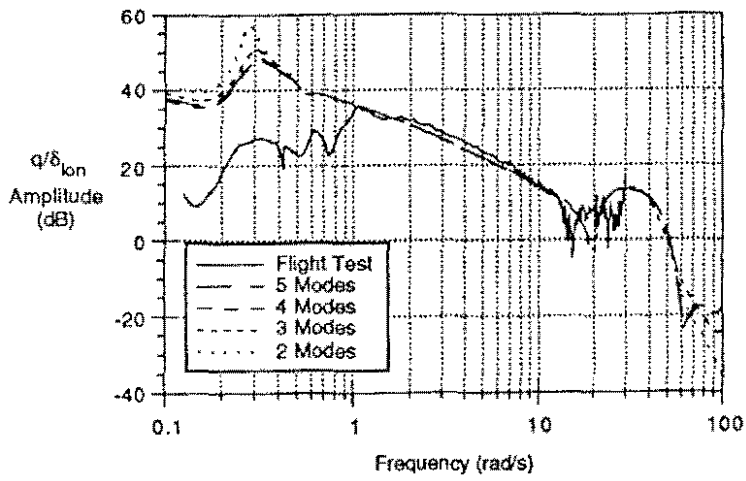


Figure 4: Pitch rate frequency response to longitudinal cyclic input δ_{lat} .

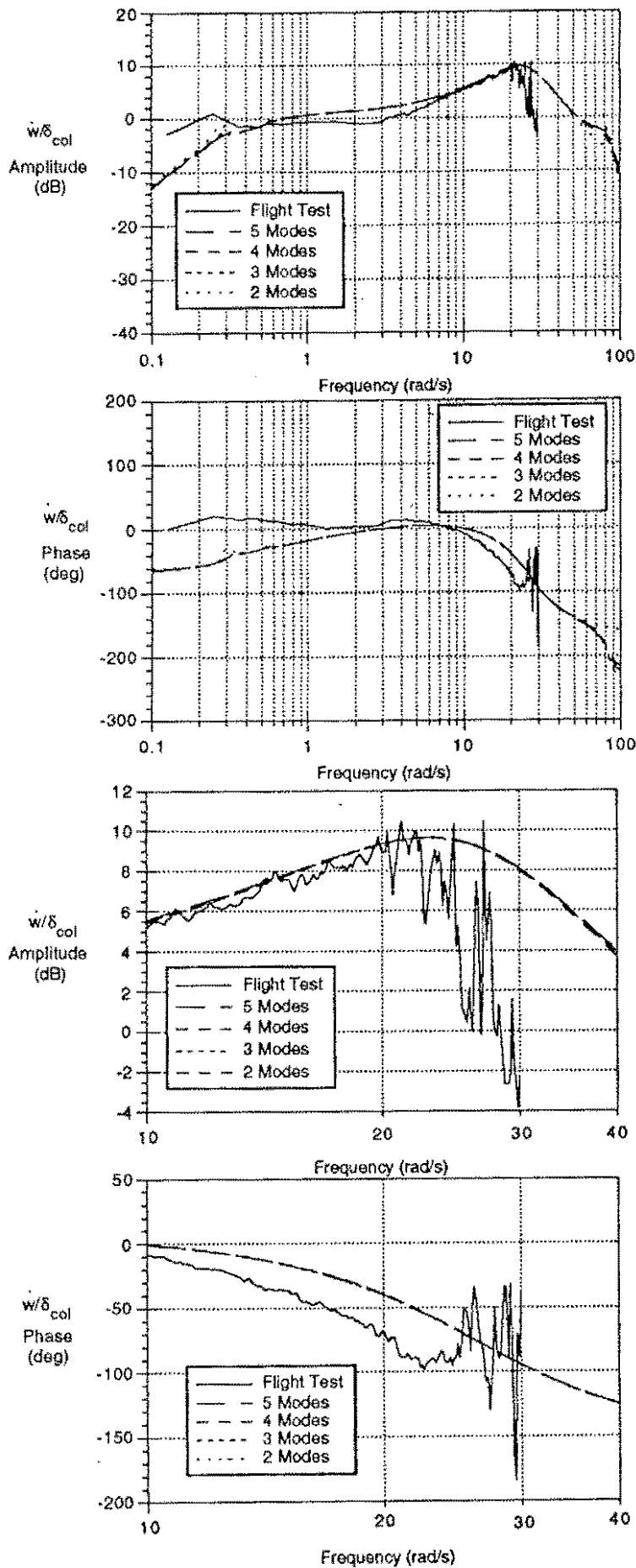


Figure 5: Heave acceleration frequency response to collective pitch input δ_{col} .

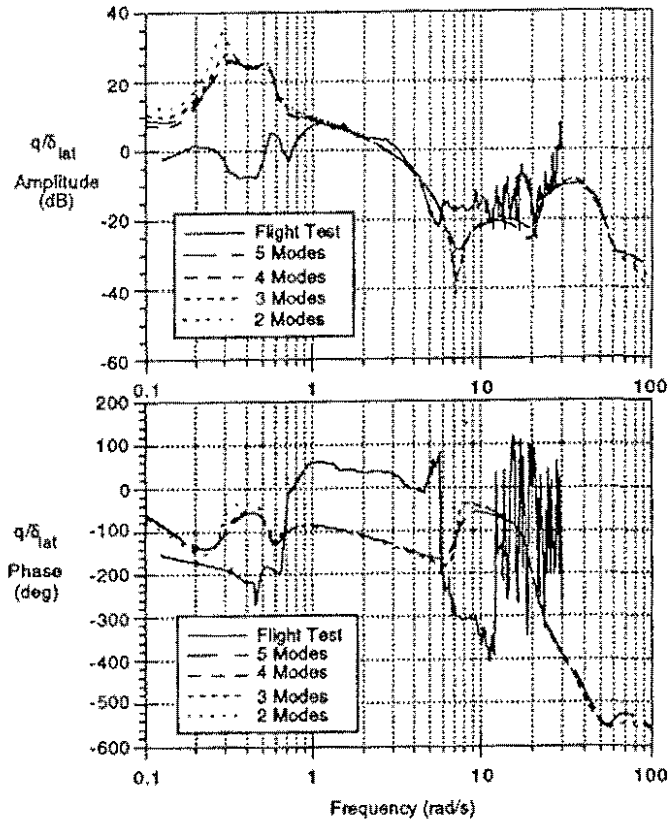


Figure 6: Pitch rate frequency response to lateral cyclic input δ_{lat} .

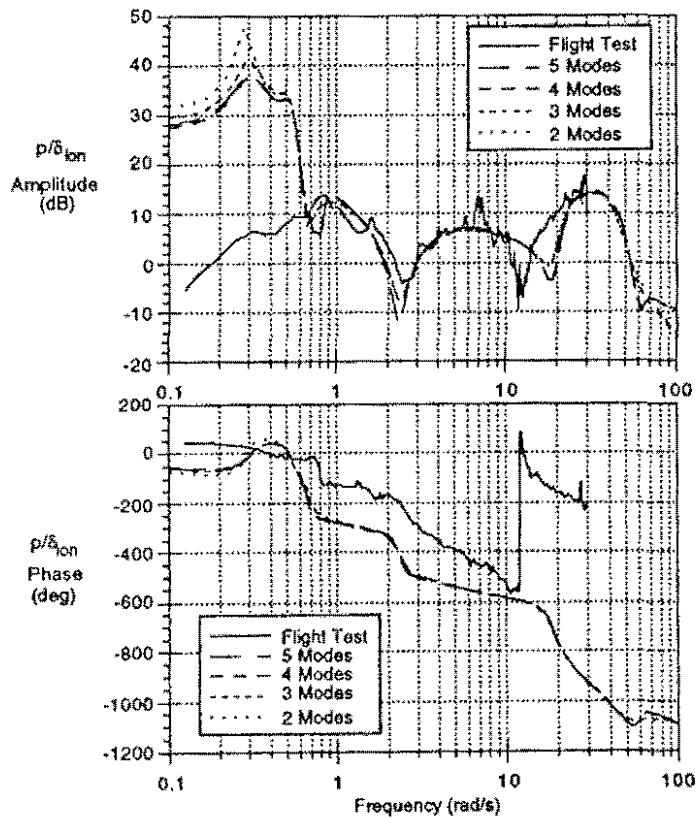


Figure 7: Roll rate frequency response to longitudinal cyclic input δ_{lon} .